AERODYNAMIC HIGH-PRESSURE HYDROGEN CFRP VESSELS WITH INCREASED STORAGE ENERGY DENSITY: METHOD FOR THE OPTIMIZATION OF A MANUFACTURABLE LAMINATE

D. Schlegel[1*], F. Schmidt[2], M. Birke[2], S. Spitzer[2] and M. Gude[2]

[1] Boysen-TUD-Research Training Group,
TUD Dresden University of Technology, Dresden, Germany
[2] Institute of Lightweight Engineering and Polymer Technology (ILK),
TUD Dresden University of Technology, Dresden, Germany
* Corresponding author (david.schlegel@tu-dresden.de)

Keywords: isotensoid, hydrogen storage, friction winding, non-cylindrical, non-geodesic filament winding, conformable pressure vessel

ABSTRACT

Hydrogen storage is one of the major challenges in the transition to hydrogen-based aviation. To store enough hydrogen with minimum storage weight, carbon fiber reinforced polymer (CFRP) high-pressure tanks in underwing pods are a promising option. Aerodynamic requirements, in addition to structural requirements, lead to advantages of an ellipsoid tank geometry over the classical cylindrical geometry. Ellipsoid hydrogen pressure vessels allow for a better utilization of the design space and therefore a higher hydrogen storage volume. During the design phase, the manufacturing process must be considered to allow for geometric adaptation of the CFRP shell while maintaining the ideal isotensoid stress state in the laminate. Friction during fiber placement allows a deviation from the geodesic filament path in the filament winding process to increase the degree of freedom for the geometry of the vessel. Analytical modelling tools are developed to calculate the required friction coefficient for the isotensoid design of a given ellipsoid geometry. The manufacturing and material parameters are then adjusted and experimentally verified to facilitate this isotensoid design. The analytical methodology is validated by finite element modelling of the winding process and physical manufacturing trials.

1 INTRODUCTION

The strive for being a climate neutral continent, as outlined in the European Green Deal, demands for environmental and climate friendly propulsion solutions in transport and logistics. Especially hydrogen is seen as a longer-term option to decarbonize the aviation industry [1]. Gaseous hydrogen is a viable option for small aircrafts and short flights to supplement the cryogenic solution to store enough hydrogen for long-distance flights. High-performance storage solutions using high-pressure tanks in lightweight design ensure that the energy is available for fuel cells, combustion engines or combinations of both. Thereby, hydrogen is stored at e.g. 350, 700 or 1000 bar. CFRPs with their outstanding direction-dependent and adjustable properties are predestined for use in such high-performance storage systems. Thereby, the fibers are isotensoid and geodesical placed in the pressure-load bearing CFRP-shell of the tank.

1.1 Isotensoid filament-wound composite pressure vessels

For high performance composite pressure vessels, the most established design consists of a cylindrical middle section with two specifically shaped end domes. Typically, these are tanks of type 4, which means the design uses a polymer liner and an outer CFRP-shell (cf. Figure 1). Though different manufacturing methods are used or were researched (e.g. braiding [2]), filament winding is the most spread option. To achieve a low structural mass with this technology, an isotensoid topology is desirable. For that purpose, the geometry of the domes have to be defined in such a way that the (geodesic) winding process allows the fabrication of a composite laminate with uniformly stressed fibers while the vessel is under pressure [3; 4]. This allows for a sufficient high gravimetrical density, i.e. the amount of hydrogen as a percentage of the complete filled tank mass.

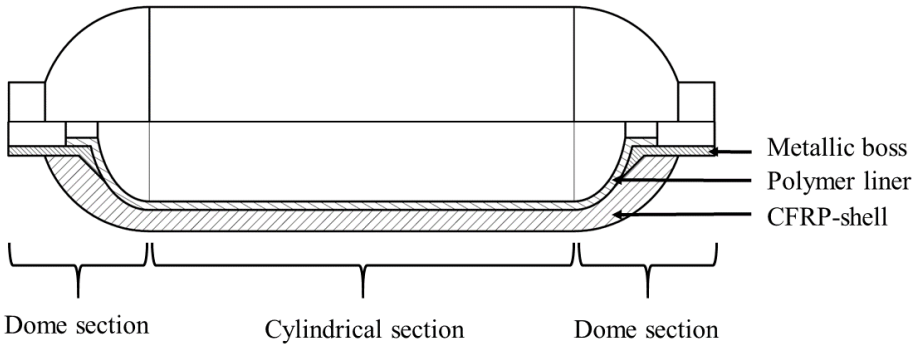

Figure 1: Schematic sketch of a type 4 pressure vessel with the typical design areas and the used materials

1.2 Ellipsoid shaped pressure vessel

For aircraft application, the question for the position of the hydrogen tanks within the airplane is of great concern. Particularly the low volumetric density of pressurized hydrogen leads to challenges for suitable integration. A more flexible, non-cylindrical design approach [5] like an ellipsoid geometry, can provide a better use of space, e.g. within aerodynamically shaped underwing gondolas (cf. *Figure 2*).

Figure 2: Aircraft with aerodynamic underwing pods as an attractive option for H_2-storage [6]

To achieve such a design a corresponding design, dimensioning and manufacturing method is necessary. This paper presents research on the theoretical basics for the fabrication of isotensoid composite layers suitable for fabrication by filament winding. This manufacturing process is well-established, ensures high quality and due to the focused non-geodesic winding, it promises sufficient freedom with respect to the necessary angle ply laminate for an isotensoid layer structure for ellipsoidal shapes.

2 METHODS

To achieve optimal performance of the ellipsoid high-pressure vessel its design, dimensioning, and manufacturing must be coordinated and finely modified. This can be achieved through a systematic engineering approach and understanding the interactions between the relevant parameters. The approach used in this paper is depicted in Figure 3. The separate processes are described in the following sections.

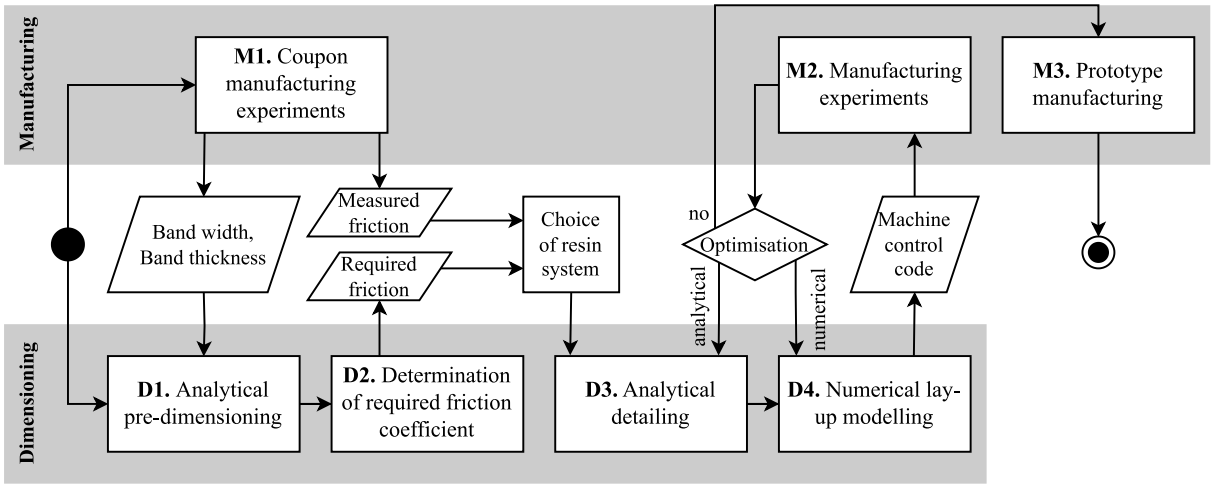

Figure 3: Flow diagram of the systematic engineering approach for an ellipsoid high-pressure hydrogen vessel

2.1 Analytical dimensioning of the isotensoid laminate

To analytically dimension the CFRP laminate of an ellipsoid pressure vessel geometry (cf. Figure 3, D1 – D3) the double-stage design process of [5] is enhanced. The calculation and optimization are implemented in PYTHON 3.10, utilizing the notation of numpy arrays. Square brackets are used to specify the indices, while the colon operator accesses all the elements of the corresponding index. The two-dimensional arrays z[i,j] and r[i,j] describe the z- and r-coordinates of the j-th laminate layer, which is defined as a fully covered filament wound $\pm\gamma$ angle-ply. Index i corresponds to the consecutive position along the z-axis of the laminate, continuing perpendicular outward from layer 0 (cf. Figure 4). Layer 0 is defined as the internal geometry of the vessel, or the winding core. Therefore, z[:,0] and r[:,0] are the two coordinate arrays, defining the internal geometry.

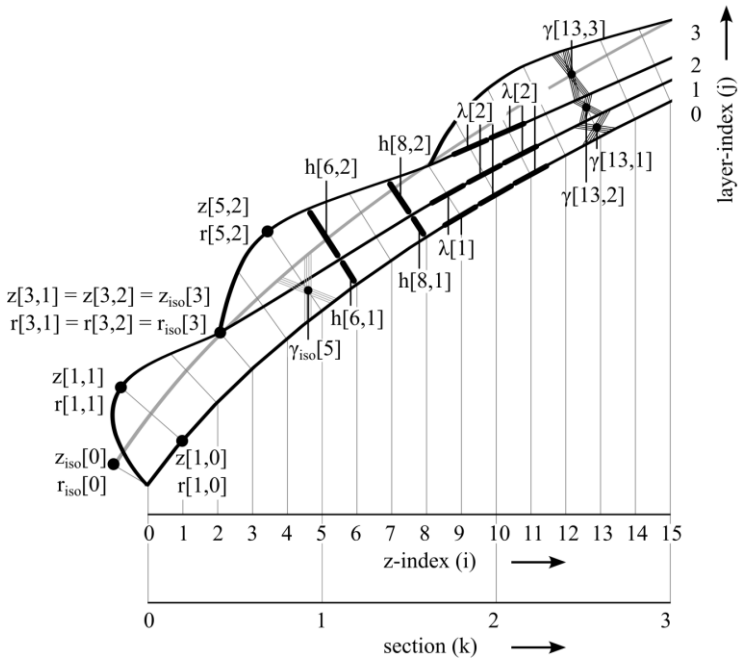

Figure 4: Indices in z-direction (i), sections (k) and for layer (j) and exemplary positions of the parameters z[i,j], r[i,j], h[i,j], γ[i,j], r_{iso}[i], λ[k]

Initially, the ideal isotensoid laminate is calculated without consideration of the manufacturing restrictions. As it assumes an angle ply laminate with a single layer, the corresponding parameters $\gamma_{iso}, h_{iso}, z_{iso}, r_{iso}$ are one-dimensional arrays with the index i. The isotensoid fiber angle of an angle ply laminate γ_{iso} is given by [5]:

$$\gamma_{iso}[i] = \arctan\left(\sqrt{2 - \frac{R_\beta[i]}{R_\alpha[i]}}\right), \tag{1}$$

where R_β is the radius of curvature in circumferential direction and R_α is the radius of curvature in longitudinal direction of the internal shell geometry.

The thickness of this angle ply laminate is calculated by [5]:

$$h_{iso}[i] = -\frac{p \cdot r[i]}{2z'[i] \cdot \overline{\sigma_1} \cdot \cos^2\gamma_{iso}[i]}\sqrt{1 + (z'[i])^2}\ , \tag{2}$$

where r is the radius, p is the internal pressure, z' = dz/dr is the gradient of the meridian and $\overline{\sigma_1}$ is the tensile strength of the unidirectional laminate in the direction of the fiber. The approach is validated in [5].

To derive a manufacturable laminate from this isotensoid target laminate an analytical winding simulation is implemented, using the mathematical formulations of WANG for the thickness prediction [7] and ZHOU'S multi-micro-cone approximation for non-geodesic winding angles [8]. The thickness prediction is based on a double formulation with a cubic spline function in the proximity of the turnaround area of the filament winding process:

$$h[\mathrm{i,j}] = A + B \cdot r[i,j] + C \cdot r[i,j]^2 + D \cdot r[i,j]^3 \qquad \text{for} \quad r_0[\mathrm{j}] \le r[i,j] \le r_{2b}[j], \tag{3}$$

and

$$h[\mathrm{i,j}] = \frac{n_R \cdot m_R \cdot t_b}{\pi} \cdot \left[\arccos\left(\frac{r_0[j]}{r[i,j]}\right) - \arccos\left(\frac{r_b[j]}{r[i,j]}\right)\right] \quad \text{for} \quad r_{2b}[j] \le r[i,j] \le R[j]\ , \tag{4}$$

where $r_0[j]$ is the radius of the respective turnaround area, t_b and w_b are thickness and width of the band and $r_{\mathrm{b}}[j] = r_0[j] + w_b$ and $r_{2\mathrm{b}}[j] = r_0[j] + 2 \cdot w_b$ [7]. The parameters n_R and m_R are the number of bands and the number of plies at the equator. Parameter n_R can be determined by [7]

$$n_R[\mathrm{j}] = \frac{2 \cdot \pi \cdot R[j] \cdot \cos\gamma_R[j]}{w_b}, \tag{5}$$

while m_R is set to 1, as each ply is to be calculated separately. Parameter γ_R describes the fiber angle at the equator and R is the radius at the equator of the respective winding ground. The coefficients A, B, C and D are determined by the following boundary conditions: Laminate thickness at the turnaround radius, continuity of thickness and curvature in $r_0 + 2 * w_b$ between the equations 4 and 5 and constant laminate volume between r_0 and $r_0 + 2 * w_b$. The predicted thickness of each layer is then added perpendicular to the previous layer, to define the new arrays z[i,j] and r[i,j]:

$$r[i,j] = r[i,j-1] + h[i,j] \cdot \sin\left(\arctan\left(r'[i,j-1]\right)\right), \tag{6}$$

$$z[i,j] = z[i,j-1] - h[i,j] \cdot \cos\left(\arctan(r'[i,j-1])\right). \tag{7}$$

The non-geodesic winding angle is calculated with the formula [8]:

$$r_i \cdot \sin(\gamma_i) = \frac{r_0 \cdot \sin(\gamma_0)}{1 - r_0 \cdot \sin(\gamma_0) \cdot \sum_{i=0}^{N-1}\left(\lambda_i \cdot \frac{z_{i+1} - z_i}{r(z_i) \cdot r(z_{i+1})}\right)}\ , \tag{8}$$

where N is the number of discrete coordinates of the meridian *z(r)*, and λ is the slippage coefficient, which must fulfill the condition $|\lambda| < \mu$. Contrary to the original publication, the slippage coefficient is included in the sum to allow for an adjustment of the non-geodesic winding angle along the z-axis [3]. It represents the amount and the direction of the friction that is being utilized in the respective coordinate z_i. The angle γ_0 is the fiber angle in the turnaround area, which must be always 90° for the filament winding process to be continuous. A compound angle $\gamma_{compound}$ corresponding to a monotropic equivalent angle ply laminate is calculated to evaluate the structural mechanics of the filament-wound laminate using the following formula [9]:

$$\sum_{i=j}^{n} \left(\frac{h}{h_j} \cdot \sin^2 \gamma_j \right) = \sin^2 \gamma_{compound} \,. \tag{9}$$

The Medium Signed Deviation (MSD), which is used as optimization criteria, is calculated by:

$$MSD = \frac{\sum_{i=k \cdot n_{section}}^{(1+k) \cdot n_{section}} (\gamma_{compound}[i] - \gamma_{iso}[i])}{n_{section}} . \tag{10}$$

The flow chart for the design and dimensioning process of the CFRP-shell, is depicted in Figure 5. Besides the internal vessel geometry, tensile laminate strength, and internal pressure, the manufacturing-dependent parameters have a significantly impact on the overall design of the vessel. Specifically, the width and thickness of the deposited filament band w_b and t_b, as well as the friction coefficient between the filament and the layer underneath μ, must be considered in the design process. The determination of those manufacturing-dependent parameters is discussed in chapter 2.3. The layer thickness at the equator is estimated to be $t_R = 2 \cdot t_b$.

To allow for an optimization of the compound fiber angle $\gamma_{compound}$, a variation of the slippage coefficient along the *z*-axis is realized. This slippage coefficient is applied to all layers in thickness direction to ensure a uniform utilization of the friction and to decrease the optimization parameters. The compound fiber angle on each point along the *z*-axis is dependent on the fiber angles and thicknesses of all layers in this point (cf. Equation (9)).

In order to enable the optimization of $\gamma_{compound}$, the calculation method of SCHLEGEL [5] is adapted so that the relevant parameters are not calculated layer by layer, but along the *z*-axis. As the thickness prediction of each wound layer is dependent on the radius of the respective winding ground *R* and the fiber angle at the equator γ_R (cf. Equation (5)). As these are unknown for all points $z(r) < z(R)$ before the equator itself, these values are guessed. The fiber angle γ_R is guessed as the geodesic fiber angle using Equation (8) with $\lambda = 0$, the known r_0 of the respective layer and the corresponding angle of 90°. The radius of the respective layer *R* is calculated as $R = R_i + i \cdot t_b$. The error due to this inaccuracy has been found to be so small that there is no need for correction.

The optimization is carried out sector wise (index k, cf. Figure 4). In the first iteration of the optimization the slippage coefficient is set to zero $\lambda[k] = 0$. The parameters of $h[i,j]$ and $\gamma[i,j]$ and $\gamma_{compound}[i]$ are calculated for all layers *j* needed to achieve the isotensoid thickness $h_{iso}[i]$, and for all indices *i* inside of the respective sector *k*. Then the MSD is calculated for $\gamma_{compound}[i]$ and $\gamma_{iso}[i]$ inside of the respective sector *k*. When $|\lambda[k]|$ is larger or equal μ, no further optimization of this sector is possible, and the calculation is carried out for the subsequent z-coordinate in the subsequent sector. If $|\lambda[k]|$ is smaller than μ, $\lambda[k]$ gets optimized for the respective sector. When the MSD is larger than the threshold ε_{MSD}, $\lambda[k]$ is increased by the amount $\Delta\lambda$. In case of the MSD being smaller than $-\varepsilon_{MSD}$, $\lambda[k]$ is decreased by the amount $\Delta\lambda$. Otherwise, no optimization is necessary, as the absolute value of the MSD is smaller than the threshold ε_{MSD}, and therefore, the angle deviation is within the acceptable range.

The calculation of the section is then repeated with the adjusted slippage coefficient. Once all coordinates are calculated, the optimization is completed. As the compound fiber angle naturally fluctuates to some extend around the turnaround areas of layers, an optimization without the sections would lead to the slippage coefficient to fluctuate between - μ and μ and thus, would not fully utilize the potential of the non-geodesic winding process. The suitable length of the section $n_{section}$, was set to cover around $1.5 \cdot w_b$. This effect can be better understood in chapter 3.3 and Figure 9.

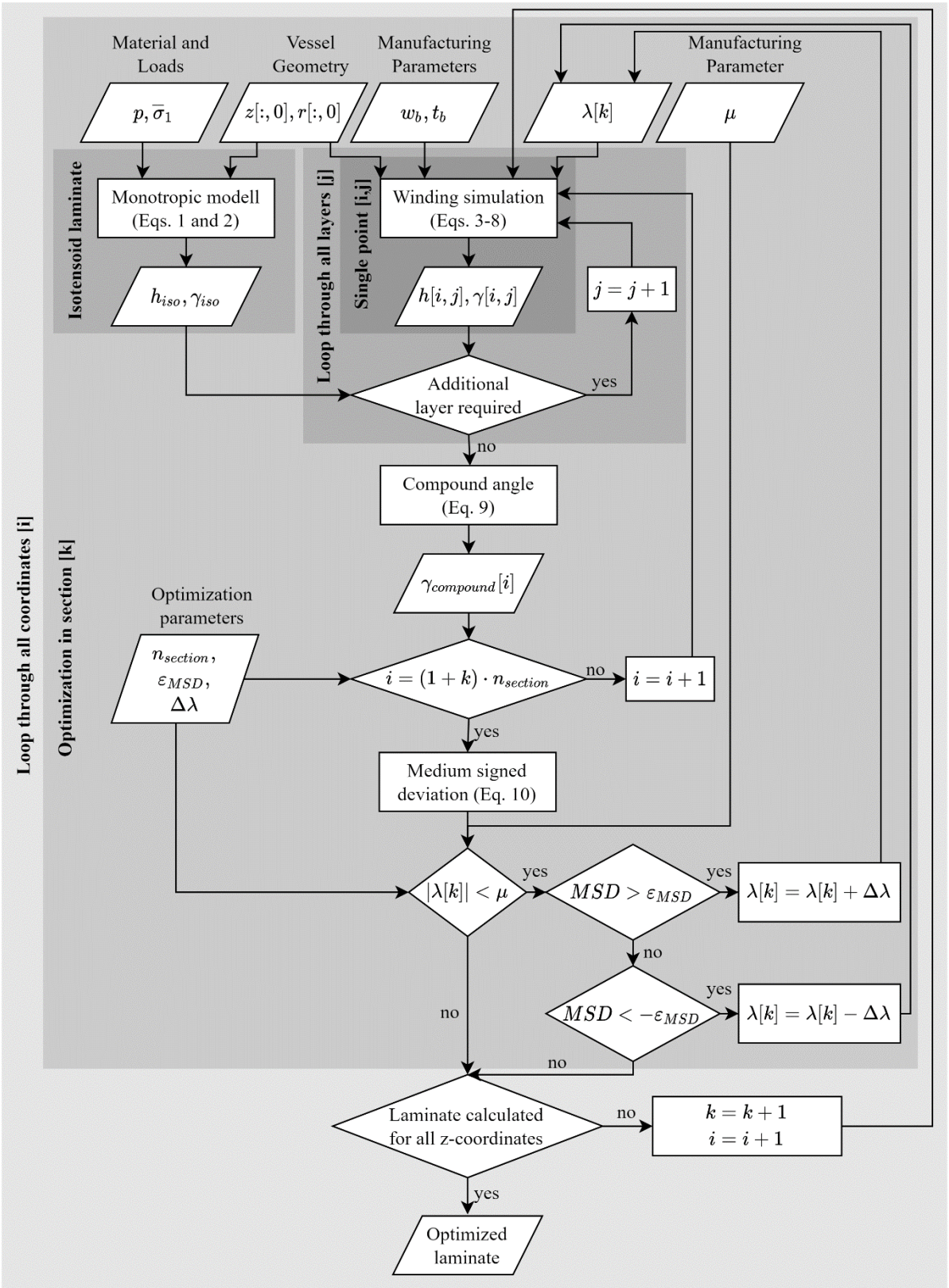

Figure 5: Iterative dimensioning of a filament wound isotensoid CFRP laminate for the ellipsoid high-pressure vessel

2.2 Numerical winding simulation

The method to generate a winding program in accordance with the analytic simulation tool uses CADWIND 9.6.4.1 (cf. Figure 3, D4). To achieve a winding program, it is necessary to create a digital model of the winding core in the first place. For this specific case study, the outer surface of the liner, which acts as a winding core for the ellipsoid type 4 vessel, is modelled with a CAD-Software and subsequently divided into frames with specific length in axial direction.
To use the data generated by the analytical winding tool introduced above, the output datapoints for each layer and axial position need to be postprocessed. The relevant data is converted into CADWIND winding parameter (*.WIP) data files, wherein every frame gets its fiber orientation assigned that was previously determined by the analytical winding simulation.
By reading in the modified *.WIP files directly into CADWIND and adding further for the winding process relevant parameters, such as for example the maximum usable friction factor, the winding path for one cycle can be generated by non-geodesic winding as shown in Figure 6.

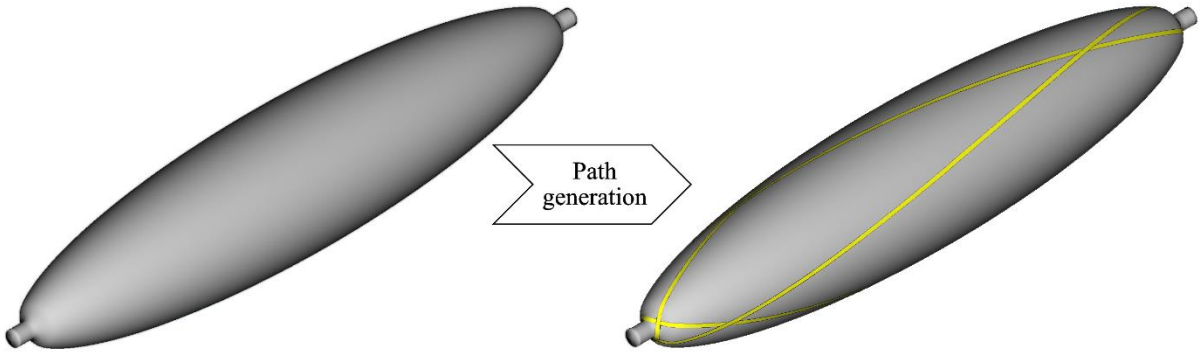

Figure 6: Digital winding core before (left) and after winding path generation (right) in CADWIND

2.3 Experimental determination of relevant parameters

The relevant manufacturing parameters for the analytical dimensioning are the band width w_b, the band thickness t_b and the friction coefficient μ (cf. Figure 5). Winding experiments are carried out with the process parameters expected for the manufacture of the actual ellipsoidal vessel (cf. Figure 3, M1). These parameters are determined by winding on a cylindrical winding core with a similar outer diameter while using the same winding eye and filament guides that will be used for the winding of the ellipsoid vessel.
The bandwidth of the applied fiber band w_b is measured by winding on the core with subsequent optical measurements. The resulting band thickness t_b is calculated under the assumption of volume consistency:

$$t_b = \frac{n_{Rovings} \cdot n_{tex}}{w_b \cdot \rho_{CF} \cdot \varphi}, \tag{11}$$

where $n_{Rovings}$ is the number of rovings that are deposited simultaneously and compose the winding band, n_{tex} is the tex size and ρ_{CF} the density of the used carbon fiber rovings. The fiber-volume fraction (FVF) φ of the wound structure depends on several variables, such as the fiber winding tension [10] and the layer position within the ply lay-up [11]. For the first preliminary study a constant FVF of 60 % is assumed.
The friction coefficient depends largely on the winding ground of the deposited band. As a rough polymeric winding ground offers high friction coefficients [12], the 3D-printed core is assumed to have a higher friction coefficient than a previously wet-wound layer. Therefore, an experimental measurement of the friction coefficient μ is only carried out for the deposition of a fiber band on a previously wet-wound layer.
A closed hoop layer is deposited on the winding core, followed by the deposition of a band along a non-geodesic winding path. This non-geodesic path is programmed with CADWIND to fully utilize a given

friction coefficient μ. The experiment is started with a low friction coefficient of 0.1 which is then incrementally increased until visible slipping of the fibers occurs (cf. Figure 7). The last iteration without fiber slipping determines the maximum friction coefficient for the specific material system. To investigate the influence of the resin viscosity on the friction factor, several resin systems are tested with this method in chapter 3.1.

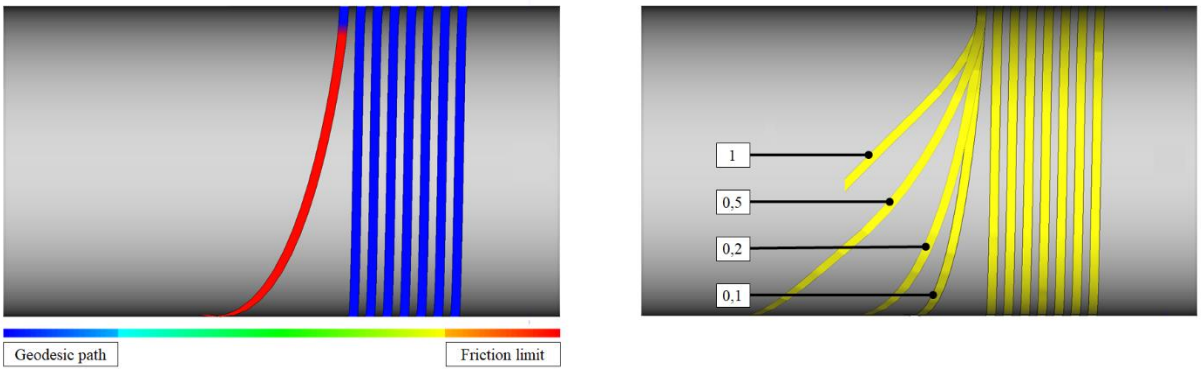

Figure 7: Usage of friction limit (left) and deviation of the winding path in dependence of underlying friction coefficient created by CADWIND (right)

3 RESULTS

3.1 Winding Experiment Results

To determine the bandwidth of the fiber bands for the engineering process M1 (cf. Figure 3), the method described in chapter 2.3 is applied. The winding is performed with 4 rovings of Tenax™-E ITS50 F23 24K 1600tex D by Teijin, each with a carbon fiber density of 1,8 g/cm^3 [13]. Hoop layers were applied on the winding core and measured afterwards. The detected bandwidth of 9 mm results in accordance with equation 11 to an approximated layer thickness of 0.67 mm. These results are then implemented into the analytical winding tool and are used for the analytical pre-dimensioning of the ply lay-up.
The determination of the achievable friction coefficients is performed as described in chapter 2.3 with incremental friction coefficient increases of 0.005. The evaluated resin systems are:

1. Araldite® LY556 /Aradur® 917/ Accelerator DY 070 by Huntsman Advanced Materials,
2. Resin XB 3515/ Aradur® 1571/ Accelerator 1573 by Huntsman Advanced Materials,
3. HexFlow® RTM6 by Hexcel®.

Fiber slipping is detected visually. Figure 8 depicts the fiber band path before (dotted blue) and after slippage (red).

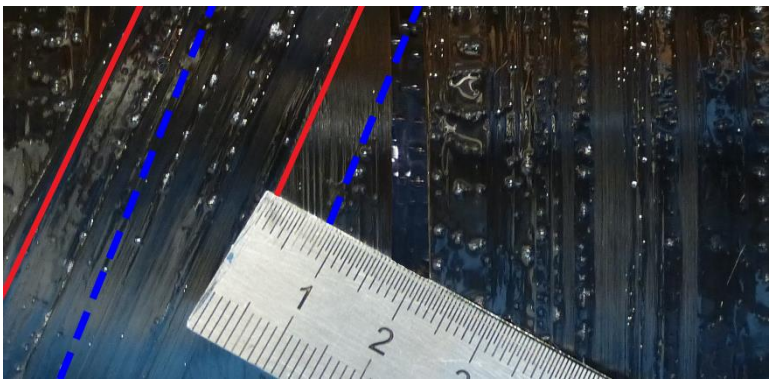

Figure 8 Fiber path before (dotted blue) and after slippage (red)

The test results for the friction coefficients are shown in Table 1.

Resin System	Viscosity at 65 °C in mPas	Friction coefficient	Impregnation quality
Araldite® LY556 /Aradur® 917/ Accelerator DY 070	< 75 [14]	0.12	Good
Resin XB 3515/ Aradur® 1571/ Accelerator 1573	30000 - 40000 [15]	> 0.19	Very poor
HexFlow® RTM6	> 700 [16]	0.17	Poor

Table 1: Properties and test results of the resin systems for non-geodesic winding

Although RTM6 and Resin XU3508/Hardener XB3473 achieved high friction coefficients, those systems are not suitable for the current state of the art wet filament winding process, as the achievable impregnation quality with those resin systems is too low. Even preheating of the resin bath to up to 60 °C does not improve the impregnation properties of those resin systems sufficiently. In contrast to these results, the resin system Araldite® LY556 /Aradur® 917/ Accelerator DY 070 achieves a good impregnation quality with a lower friction coefficient of 0.12. These results are used for the further analytical dimensioning of the ellipsoid vessel.

3.2 Analytical dimensioning of the ellipsoid

To choose a suitable resin system, the parameters w_b and t_b from chapter 3.1 are used for the analytical winding simulation according to chapter 2.1. Then the minimal friction coefficient needed for a good accordance between $\gamma_{compound}$ and $\gamma_{isotensoid}$ is iteratively evaluated (cf. Figure 3, D3).

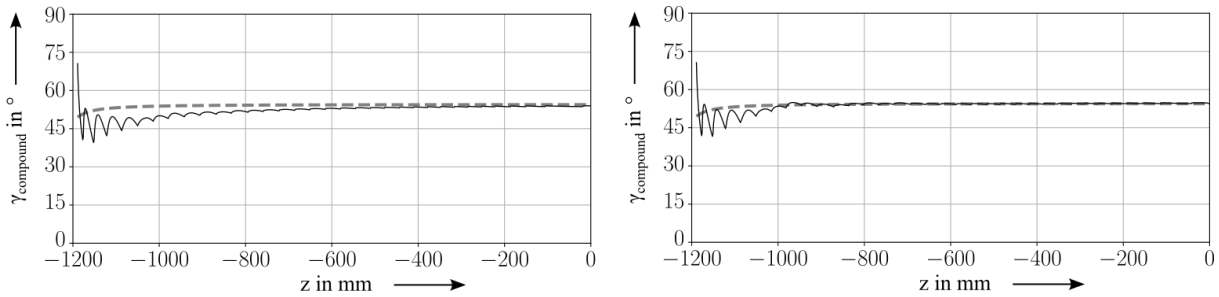

Figure 9: Geodesic compound fiber angle (left), non-geodesic compound fiber angle with a friction coefficient of 0.05 (right) in comparison to the isotensoid fiber angle (grey dotted line)

Figure 9 shows the resulting compound fiber angles for the optimized laminate according to the calculation method in Figure 1 for geodesic winding (left) and non-geodesic winding with a friction coefficient of 0.05 (right). The geodesical wound structure shows a deviation of 7° at $z = -1100\ mm$. This is already decreased significantly to 4° by assuming a friction coefficient of 0.05, also for $-1000\ mm < z < 0\ mm$ the alignment between $\gamma_{compound}$ and $\gamma_{isotensoid}$ is very close.
By assuming a friction coefficient of 0.1, the deviation can be almost eliminated (cf. Figure 10, bottom left). The maximal slippage coefficient resulting from the optimization is 0.0875 (cf. Figure 9, bottom right). A further increase in friction would not benefit the design of the pressure vessel and the resin system Araldite® LY556 /Aradur® 917/ Accelerator DY 070 is chosen for the manufacturing of the pressure vessel. The resulting laminate layup is depicted in Figure 9, top left and the fiber angle of all separate layers are depicted in Figure 9, top right (cf. Figure 3, D3).

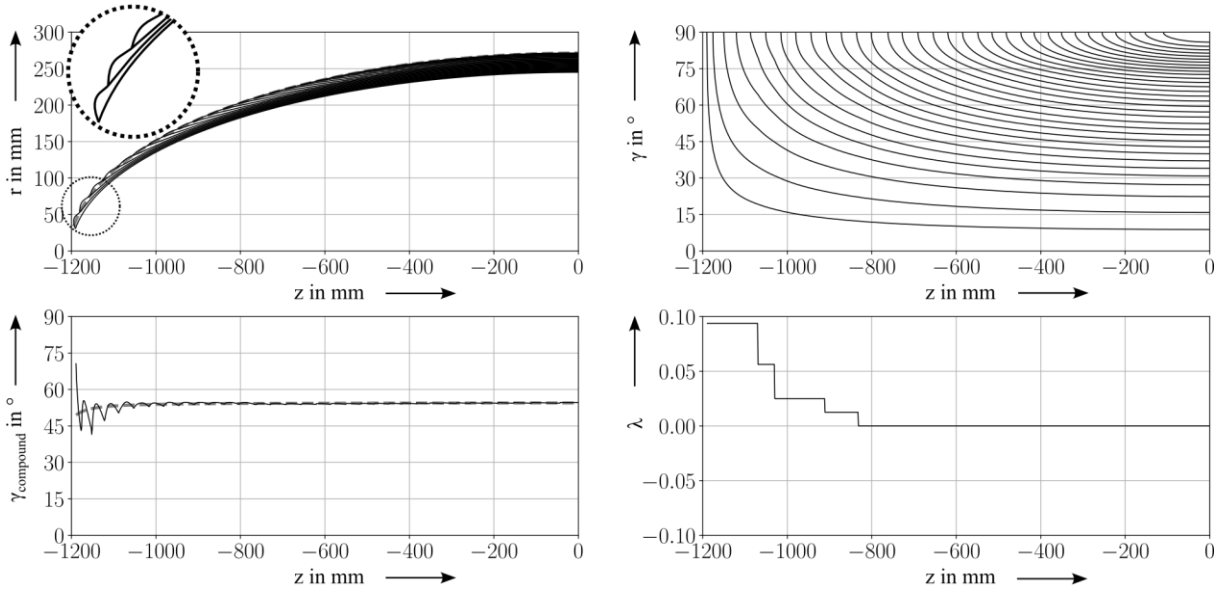

Figure 10: Fiber layup (top left), fiber angles of separate laminate layers (top right), non-geodesic compound fiber angle with a friction coefficient of 0.1 (bottom left), optimized slippage coefficient (bottom right)

3.3 Numerical lay-up creation based on the analytical dimensioning

The analytically detailed laminate (cf. Figure 10) is now transferred to a numerical model (cf. Figure 3, D4). Each layer is generated by transferring the winding path from the analytical winding tool to CADWIND according to the method described in chapter 2.2. To achieve a completely closed layer, a suitable winding pattern is chosen. After each layer, the winding core is updated to account for the geometrical change, due to the thickness buildup of the fibers. Then the next layer is generated. Figure 11 shows models of the bare core (left) with selected fiber layers (middle, right). Based on the layer information, a machine specific winding program can be created within CADWIND.

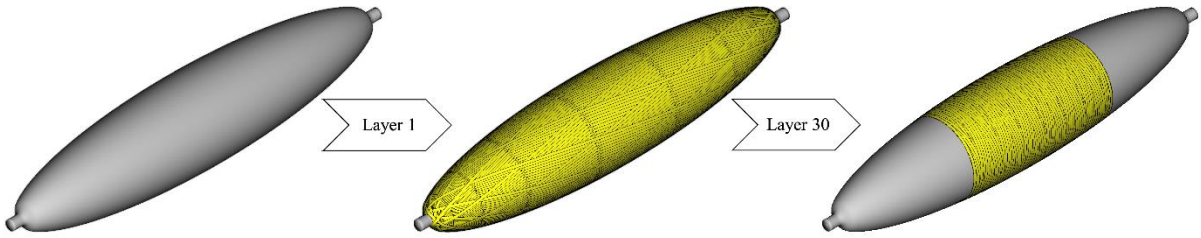

Figure 11: Empty winding core (left), virtually applied first layer (centre) and 30th layer (right)

4 CONCLUSIONS AND OUTLOOK

An optimization method for the ideal isotensoid laminate of an ellipsoid pressure vessel is proposed. The interactions between manufacturing, design and dimensioning were analyzed by means of manufacturing experiments, analytical and numerical modelling.

To derive the relevant manufacturing parameters for the dimensioning process a method to measure the friction coefficient of a wet-wound fiber deposition is proposed. The analytical dimensioning method is based on the two-stage process of [5]. First, an ideal isotensoid laminate is calculated. It is then analytically transferred to a laminate design, manufacturable by means of non-geodesic filament winding. This analytical method was extended by an optimization method, to enhance accuracy, and to distribute the slippage coefficient evenly along the thickness of the laminate. It is shown that a relatively low friction coefficient of 0.1 is sufficient to manufacture the calculated design. The successful transfer of the analytically calculated laminate to the FE-software is a validation of the feasibility of the

analytical method.
Based on the winding experiments and the analytical design method, a resin system was chosen for the further development process. The laminate was then detailed analytically, transferred to a numerical layup, and translated to machine control. The first full laminate layer of the ellipsoid vessel was carried out (cf. Figure 12), validating the manufacturability of the design.

Figure 12: First filament wound layer of the ellipsoid pressure vessel

Some potentials for enhancing the design of the vessel were also discovered. The FVF is varying in the manufactured laminate, which could be considered in the analytical winding simulation. To reduce this FVF variation the winding patterns can be further optimized. A detailed evaluation of the fiber angles and thickness distribution of the analytically, numerically, and physically wound laminates could increase the accuracy of the design and dimensioning process.
To carry out a strength analysis of the filament wound ellipsoid pressure vessel, the modelled layer can be imported from CADWIND into a FE software. This allows to identify potential issues with the design, that are neglected in the analytical dimensioning, allowing for a detailed strength analysis of the boss area, also including the liner. After numerical strength analysis and further design iterations, the ellipsoid high-pressure vessel will be manufactured, and a burst test will be carried out.

ACKNOWLEDGEMENTS

The corresponding author thanks the Boysen-TU Dresden-Research Training Group for the financial support that has made this publication possible. The Research Training Group is co-financed by Technische Universität Dresden and the Friedrich and Elisabeth Boysen Foundation.
The project H2GA is being funded under the directive on the promotion of light and heavy commercial vehicles with alternative, climate-friendly drive systems and the associated fueling and charging infrastructure (KsNI) with a total of 4.186.128,00 € from the Federal Ministry of Digital and Transport. The funding guideline is coordinated by NOW GmbH, applications are approved by the Federal Office for Goods Transport.

REFERENCES

[1] European Commission. (2020). *A hydrogen strategy for a climate-neutral Europe.* European Commission. https://eur-lex.europa.eu/legal-content/EN/TXT/?uri=CELEX:52020DC0301
[2] Gruhl, A., Lanzl, T., Friedrich, M., Hofmann, F. & Feist, M. Verfahren zur Herstellung eines Druckspeichers sowie Druckspeicher(DE 10 2013 113 208 A1)
[3] Vasiliev, V. V. & Jones, R. M. (2009). *Composite Pressure Vessels: Analysis, Design, and Manufacturing*. Bull Ridge Pub. https://books.google.de/books?id=oF-oWPmKU4UC

[4] Vasiliev, V. V., Krikanov, A. A. & Razin, A. F. (2003). New generation of filament-wound composite pressure vessels for commercial applications. *Composite Structures*, *62*, 449–459

[5] Schlegel, D., Spitzer, S., Birke, M., Lange, A. & Gude, M. (2022). Aerodynamic High-Pressure Hydrogen CFRP Vessels with Increased Storage Energy Density for Green Aviation: Novel Design and Dimensioning Method. In *SAMPE Europe 22 Conference.* Symposium im Rahmen der Tagung von Society for the Advancement of Material and Process Engineering Europe, Hamburg (Germany)

[6] Lange Research Aircraft GmbH. (2022). *Übertragung automobiler H2-BZ-Technologie in den Demonstrator Antares E2* [Press release]. https://www.now-gmbh.de/projektfinder/h2ga/

[7] Wang, R., Jiao, W., Liu, W. & Yang, F. (2011). Dome Thickness Prediction of Composite Pressure Vessels by a Cubic Spline Function and Finite Element Analysis. *Polymers and Polymer Composites*, *19*(2-3), 227–234

[8] Zhou, J., Chen, J., Zheng, Y., Wang, Z. & An, Q. (2017). Dome shape optimization of filament-wound composite pressure vessels based on hyperelliptic functions considering both geodesic and non-geodesic winding patterns. *Journal of Composite Materials*, *51*(14), 1961–1969

[9] Schürmann, H. (2007). *Konstruieren mit Faser-Kunststoff-Verbunden* (2., bearb. und erw. Aufl.). Springer.

[10] Cohen, D. (1997). Influence of filament winding parameters on composite vessel quality and strength. *Composites Part A: Applied Science and Manufacturing*, *28*(12), 1035–1047

[11] Banerjee, A., Sun, L., Mantell, S. C. & Cohen, D. (1998). Model and experimental study of fiber motion in wet filament winding. *Composites Part A: Applied Science and Manufacturing*, *29*(3), 251–263

[12] Koussios, S. & Bergsma, O. K. (2006). Friction Experiments for Filament Winding Applications. *Journal of Thermoplastic Composite Materials*, *19*(1), 5–34

[13] Teijin Carbon Europe GmbH. (2021). *Product data sheet Tenax™-E ITS50 F23 24K 1600tex D.*

[14] Huntsman Advanced Materials. (2017). *Product data sheet Araldite® LY 556/ Aradur® 917-1/ Accelerator DY 070.*

[15] Huntsman Advanced Materials. (2009). *Product data sheet Resin XB 3515/ Aradur® 1571/ Accelerator 1573.*

[16] Hexcel Corporation. (2022). *Product data sheet HexFlow® RTM6.*